Mon. Not. R. Astron. Soc. **000**, 1–?? (2009) Printed 3 April 2009 (MN LATEX style file v2.2)

Chromospheric changes in K stars with activity

Mariela C. Vieytes⋆, Pablo J. D. Mauas, and Rodrigo F. Díaz †
Instituto de Astronomía y Física del Espacio,
CC. 67 Suc. 28 (1428)Buenos Aires, Argentina

Accepted . Received ; in original form

ABSTRACT
We study the differences in chromospheric structure induced in K stars by stellar activity, to expand our previous work for G stars, including the Sun as a star. We selected six stars of spectral type K with $0.82< B-V <0.90$, including the widely studied Epsilon Eridani, which have a wide variety of magnetic activity levels. We computed chromospheric models for the stars in the sample, in most cases in two different moments of activity. The models were constructed to obtain the best possible match with the Ca II K and the Hβ observed profiles. We also computed in detail the net radiative losses for each model to constrain the heating mechanism that can maintain the structure in the atmosphere. We find a strong correlation between these losses and S_{CaII}, the index generally used as a proxy for activity, as we found for G stars.

Key words: radiative transfer - stars: atmosphere - stars: activity

1 INTRODUCTION

Solar and stellar chromospheric models have been developed to study the dependency of chromospheric plasma parameters with height and temperature. **The best known examples are the models for the solar atmosphere computed by E. Avrett and his co-workers, in particular model C for the average quit Sun by Vernazza et al. (1981), and later modified by Fontenla et al. (1993)**

In several cases, these models were used to characterize changes due to activity and spectral type. For example, Kelch et al. (1979) studied a sample of eight main-sequence stars ranging in spectral type from F0 to M0, some of which were of similar spectral type and different levels of chromospheric activity. They computed the photospheric structure starting from a radiative equilibrium model for the $T_{\rm eff}$ of each star and fitting the Ca II K line wings. The chromosphere was built using the emission core of the Ca II K line. To estimate the radiative cooling rate in the K line they used the K_1 index (Linsky & Ayres 1978), which is calculated as the difference between the integrated flux inside the two K_1 minima of the Ca II K line and the corresponding flux for the model in radiative equilibrium.

Their results showed that non-radiative heating is important in the lower photosphere of all the late-type stars under study. They found that the value of the K_1 index and the temperature gradient in the lower chromosphere of these stars, as a function of $T_{\rm eff}$, divides active and inactive stars, and that the cooling rate in chromospheric lines decreases with $T_{\rm eff}$. Regarding the chromospheric structure, they found that the temperature minimum moves outward, to lower values of column mass density, with decreasing magnetic activity, *i.e.* with decreasing non radiative heating in the lower chromosphere.

Semi-empirical models of the dM star AD Leo in its quiescent state and during a flare were built by Mauas & Falchi (1994) and Mauas & Falchi (1996) respectively. Subsequently, models of two "basal" (*i.e.* inactive) stars of the same spectral type, Gl588 and Gl628, were constructed by Mauas et al. (1997).

In a previous paper (Vieytes et al. 2005, hereafter Paper I), we computed chromospheric models for a sample of dwarf stars of spectral type G, including the Sun as a star, **using the FAL models by Fontenla et al. (1993) as a starting point**. Our purpose was to study the changes in chromospheric structure induced by magnetic activity. The stars we modeled were chosen to have similar colors than the Sun, and therefore similar photospheric structures, but different chromospheric activity levels, probably due to different ages and/or rotation periods. These stars can be considered as solar analogues, since they share several characteristics with the Sun.

To extend our research to cooler stars and to study how the chromospheric structure changes with spectral type and chromospheric activity, in this paper we perform a study similar to the one in Paper I for several dwarfs of spectral

⋆ E-mail:mariela@iafe.uba.ar
† Visiting Astronomer, Complejo Astronómico El Leoncito operated under agreement between the Consejo Nacional de Investigaciones Científicas y Técnicas de la República Argentina and the National Universities of La Plata, Córdoba and San Juan.

type K, selected with similar colour, *i.e.* similar photospheric structure, and with different levels of magnetic activity.

As the base for our sample we selected one of the most studied K stars, Epsilon Eridani (HD 22049), which is an active star of spectral type K2 V ($B-V$=0.88), with $T_{\rm eff}$ = 5110 K. This star has been widely studied because it is one of the ten nearest stars. It has two planets and a belt of dust particles around it, which has been compared to the Kuiper belt in the Sun. These facts make this stellar system resemble our own Solar System.

Several chromospheric models have been computed for this star. Kelch (1978) modeled the lower chromosphere to match the Ca II K line profile and integrated fluxes of the Mg II h and k lines. Using observations of the ultraviolet lines of C II, Mg II, Si II and Si III from the IUE satellite, Simon et al. (1980) obtained a model for Epsilon Eridani, which also reproduces hydrogen line profiles not fitted by Kelch's model. The thermal structure of this model has the onset of the transition zone deeper in the chromosphere and a lower temperature in the plateau than Kelch's model.

Another chromospheric model for Epsilon Eridani is the one by Thatcher et al. (1991), who fitted the Ca II K line, the infrared triplet lines of Ca II, the Na D doublet, Hα and Hβ. Finally, Jordan et al. (2005), using ultraviolet observations from STIS and FUSE, developed a new semiempirical model for the upper chromosphere and lower transition region of this star keeping the photosphere and lower chromosphere of Thatcher et al. (1991).

This Paper is arranged as follows: we present our stellar sample and discuss the observational data in §2. In §3 we describe the models and show the results. In §4 we compute the energy requirements to sustain the chromosphere, and compare the results with those obtained for G stars in Paper I. Finally, in §5 we discuss the results.

2 OUR STELLAR SAMPLE

The largest observational study of chromospheric activity is the one started in 1966 at the Mount Wilson Observatory, which at present includes more than 2200 stars in the spectral range between F and early K. As indicator of chromospheric stellar activity, they use the $S_{\rm CaII}$ index, which is the ratio of the fluxes in the H and K line cores and two nearby reference windows 20 Å wide (Vaughan et al. 1978). The emission in the cores of these lines increase with increasing chromospheric activity, *i.e.* with increasing surface magnetism. In this work we used the same activity indicator.

To select the stars in our sample, we require that $0.82 < B–V < 0.90$, a colour similar to ε Eri, and that the magnetic activity levels are different. All the stars are part of the library of southern late-type dwarfs published by Cincunegui & Mauas (2004, hereafter CM04).

The stellar parameters of the stars in our sample are listed in Table 2. In the third column we list the spectral type, in the fourth to sixth columns we indicate the colour index $B-V$, $T_{\rm eff}$ and the metallicity. In column 7 we show the mean values of the $S_{\rm CaII}$ index obtained at the Cerro Tololo InterAmerican Observatory (Henry et al. 1996), and in columns 8 and 9 the maximum and minimum $S_{\rm CaII}$ obtained from our spectra (see Cincunegui et al. 2007 for details on how this index is obtained) **and from the models we built in this paper**. Finally, in the last two columns of Table 2 we include the observing dates of each spectrum used in the present work.

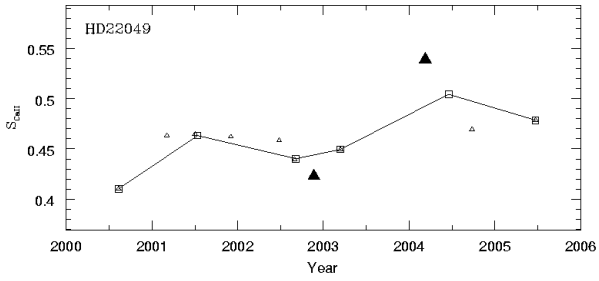

Figure 1. $S_{\rm CaII}$ for each observation for ε Eri in our library. The open triangles are the values for the different observations, the squares indicate the annual averages, and the largest full triangles show the two spectra modeled in this paper.

The observations were made at the 2.15 m telescope of the Complejo Astronomico El Leoncito (CASLEO), located in San Juan, Argentina. They were obtained with a REOSC spectrograph designed to work between 3500 and 7500 Å and a 1024 x 1024 pixel TEK CCD as detector. The spectral resolution ranges from 0.141 to 0.249 Å per pixel ($R = \lambda/\delta\lambda \simeq 26400$). We refer the reader to CM04 for more details on the observations and the data reduction.

For all the stars, we have several spectra obtained in different observing runs. To study the differences in atmospheric structure with activity level, in this paper we consider, in most cases, two spectra for each star, chosen between those with the better signal to noise ratio. Generally we selected the spectra showing the lowest and the highest levels of activity, except for HD 177996 and HD 37572, for which the least active spectra are very similar to the most active ones of HD 22049 and HD 17925 respectively. In this way, we built 10 different models. It is important to note, given the dependence of activity level with the observation time, that all the line profiles used to build the models are simultaneous.

In Figure 1 we show the $S_{\rm CaII}$ index of ε Eri obtained from our observations (open triangles). The two spectra modeled in this paper are represented by full triangles. The difference in the Ca II K line flux between the maximum and minimum is 17%. With squares we also present the annual average of the $S_{\rm CaII}$ index. For details on the variability of ε Eri, see Buccino & Mauas (2008).

3 THE CHROMOSPHERIC MODELS

For each star we built a different chromospheric model, assuming one-dimensional, plane-parallel atmospheres. We simultaneously solved the equations of hydrostatic equilibrium, radiative transfer and statistical equilibrium, using the computer code Pandora. A description of this code can be found in Avrett & Loeser (2003).

For a given distribution of temperature with height, we self-consistently computed non-LTE populations for 15 levels of H, 13 of He I, 6 of He II, 15 of Fe I, 8 of Ca I, 5 of Ca II, 7 of Mg I, 6 of Mg II, 21 of Si I, 8 of Na I and 6 of Al I. The atomic models we used for H and Ca II are described

Table 1. The stellar sample. Columns 3 to 6 list the stellar parameters (from Perryman et al. 1997, and from Cincunegui & Mauas 2004). The next three columns give the $S_{\rm CaII}$ measured by Henry et al. (1996) at CTIO and by Cincunegui & Mauas (2004) at CASLEO, both converted to Mount Wilson $S_{\rm CaII}$ **compared whit $S_{\rm CaII}$ calculated from our models**; and the last two columns list the observing dates for each spectrum we used.

HD (Name)	*S. type*	$B-V$	$T_{\rm eff}$(K)	[Fe/H]	$S_{\rm CTIO}$	$S^{max}_{\rm CM}/S^{max}_{\rm mod}$	$S^{min}_{\rm CM}/S^{min}_{\rm mod}$	Min	Max
17925 (V* EP Eri)	K1 V	0.86	4956	0.10	0.662	0.792/**0.584**	0.566/**0.520**	11/22/02	12/5/03
22049 (ε Eri)	K2 V	0.88	5110	-0.14	0.483	0.555/**0.468**	0.440/**0.389**	11/21/02	3/9/04
26965 (V* DY Eri)	K1 V	0.82	5203	-0.25	0.185	0.188/**0.149**	0.138/**0.147**	3/9/04	8/11/00
37572 (V* UY Pic)	K0 V	0.85	5175	—	0.952	0.703/**0.687**	0.691/—	—	11/24/04
128621 (α Cen B)	K1 V	0.90	5037	0.24	0.209	0.247/**0.180**	0.164/**0.139**	8/13/00	9/11/03
177996 (—)	K1 V	0.86	5092	—	0.861	0.821/**0.798**	0.613/—	—	6/27/02

in Mauas et al. (1997) and Falchi & Mauas (1998). The Ca II lines and Lyα were computed using Partial Redistribution, **as it has been done in previous chromospheric models(like, for example, the Vernazza et al. solar models)** .

An important element to include in this kind of modeling, in particular for the coolest stars, is the effect of bound-bound absorptions due to the numerous atomic and molecular lines present in the stellar atmosphere, referred to as line blanketing (Falchi & Mauas 1998), which plays a crucial role in determining both the emergent energy distribution and the physical structure of the atmosphere. In solar-type stars the most important effects come from neutral or single ionized metals. In even cooler stars molecular bands, as CN, CO, H_2O, etc, could dominate. In this paper, line blanketing is treated in non LTE, as explained in Falchi & Mauas (1998), assuming the source function is given by

$$S_\nu = \alpha J_\nu + (1-\alpha) B_\nu, \quad (1)$$

where B_ν is the Planck function and J_ν is the mean intensity. α is the scattering albedo, for which we used the expression given by Anderson (1989) which depends on wavelength, depth and temperature.

From the finished model, we computed the emitted profiles of Hβ and of the Ca II H and K lines, and modified the model until we found a satisfactory match with the observed profiles. As a check of the accuracy of the models, we also compared the observed computed profiles of the Mg I b and the Na I D lines for each model (Details of these features can be found in Mauas et al. 1988 and Díaz et al. 2007).

For comparison with synthetic profiles, the observations were converted to the stellar surface through

$$log(F_{surf}/f_{earth}) = 0.35 + 0.4(V + BC) + 4log(T_{eff}), \quad (2)$$

where F_{surf} is the stellar surface flux, f_{earth} is the flux observed at earth, V is the visual magnitude, BC is the bolometric correction given by Johnson et al. (1966), and $T_{\rm eff}$ is the effective temperature for each star, given in Table 2.

Of course, semiempirical models like this one are only a first approximation to the structure of stellar chromospheres, which are neither static nor homogeneous. Regarding temporal variations, we took care of picking our observations at times when no flares were present, using the method explained in Cincunegui et al. (2007). Spatial inhomogeneities characteristic of magnetically active stars, like starspots or active regions, cannot be resolved on the stellar surface. The models presented here, however, can be used as a first step to build two component models as was done, for example, by Mauas & Falchi (1996).

Faster temporal variations, like waves, cannot be reproduced with this kind of models, of course. We are also not considering possible small-scale spatial inhomogeneities like, for example, the chromospheric bifurcation proposed for the Sun by Ayres (1981), which should be produced by CO cooling. However, on one hand this cooling was probably overestimated (Mauas et al. 1990), and on the other it is probably too slow compared to atmospheric dynamics (Wedemeyer-Bohm & Steffen 2007). In any case, homogeneous models provide information on the "mean" state of the stellar atmosphere, where the different components are weighted by their effect on the emitted radiation, in particular on the spectral features under study.

3.1 Stellar parameters for ε Eri

Before building the model atmosphere, a set of atmospheric parameters has to be determined. Both the surface gravity and the metallicity are fundamental input parameters in any atmospheric model, and the effective temperature, although is not needed as input, is used in Ec. 2 to calculate the stellar surface flux needed to analyze the results.

In Table 3.1 we summarize several values of these quantities that can be found in the literature. Given the astrophysical interest on ε Eri, Drake & Smith (1993) recognized the necessity of determining these parameters with high precision and they summarized the methods used to obtain them until 1993, and the validity of these determinations. To improve these values, they determined the surface gravity, metallicity and effective temperature in a self-consistent way, comparing the equivalent widths of several Fe I, Fe II and Ca I lines with theoretical profiles from different model atmospheres. The parameters derived by Drake & Smith (1993) were used in the most recent model for ε Eri by Sim & Jordan (2005, hereafter SJ05), although they recognized that the value of $log(g)$ adopted could be too high (private communication).

The difficulty in the calculation of the surface gravity is that it is indirectly determined from the values of mass and stellar radius. Since these two parameters can be calculated more precisely for stars in binary systems, we studied another star of our sample, α Centauri B (HD 128621), pertaining to the system α Centauri AB. For close systems like this visual binary, the stellar radii and masses can be derived with an error of 1 to 10% (Guenther & Demarque 2000).

According to Cayrel de Strobel et al. (2001), the values

Table 2. Stellar characteristics for Epsilon Eridani (HD 22049) from Cayrel de Strobel et al. (2001) and Table 1 from Drake & Smith (1993).

$log(g)$	$T_{\rm eff}$	$[Fe/H]$	*Reference*
4.565	—	-0.0	Krishna Swamy (1966)
4.61	5020	-0.31	Hearnshaw (1974)
4.4	5000	-0.19	Oinas (1974)
4.5	5000	—	Kelch (1978)
4.5	5100	—	Tomkin & Lambert (1980)
4.1	5040	-0.20	Steenbock & Holweger (1981)
4.8	5000	-0.08	Burnashev (1983)
4.19	5040	-0.23	Steenbock (1983)
4.80	4990	-0.20	Abia et al. (1988)
4.61	5156	0.05	Bell & Gustafsson (1989)
4.75	5180	-0.09	Drake & Smith (1993)
4.75	5000	0.06	Mallik (1998)
4.38	5110	-0.14	Tomkin & Lambert (1999)
4.57	5104	-0.12	Zhao et al. (2002)
4.7	5135	-0.07	Bodaghee et al. (2003)
4.62	5052	-0.06	Allende Prieto et al. (2004)

of $log(g)$ found for α Cen B range from 4.51 to 4.73, with an average value of 4.60. We therefore adopted a value of $log(g) = 4.65$ for all the stars in our sample, since this value is contained in the range given by Drake & Smith (1993), considering the error in their calculation ($log(g) = 4.75 \pm 0.1$). **This same value of $log(g)$ was adopted by Ness & Jordan (2008) in their recent study of the corona and transition region of ε Eri.**

Regarding the rest of the stellar parameters, we adopted $T_{\rm eff} = 5110$ K (Tomkin & Lambert 1999), which is close to the value by Drake & Smith (1993). We adopted solar metallicity as a good approximation for ε Eri, as has been done in all the previous models for this star, since it is a young star which is probably not metal defficient. This was suggested by Krishna Swamy (1966), who built a grid of model atmospheres for ε Eri with different metallicities to fit the Ca II K line and found that using solar metallicity results in the best agreement with observations.

In the case of α Cen B, Ayres & Linsky (1976) built two models for this star assuming in one case solar metallicity and in the other an abundance twice as large. They concluded that the computed profiles of the Ca II K line differ very little and are in both cases consistent with the observations.

3.2 The model

To build the atmospheric models for ε Eri, as a first step we computed a photospheric structure capable of reproducing the observed continuum spectrum for this star. Once the photospheric model was obtained, we changed the chromospheric structure to fit the Ca II K and Hβ lines for both situations of interest, *i.e.* the maximum and minimum levels of chromospheric activity. This is the first time this sort of analysis is made.

Figure 2 shows the resulting models, which are presented in column mass for comparison with the best one-component model from SJ05 (their model B). In Figure 3 we compare the computed and observed continuum spectrum of ε Eri, and in Figure 4 and Figure 5 we show the

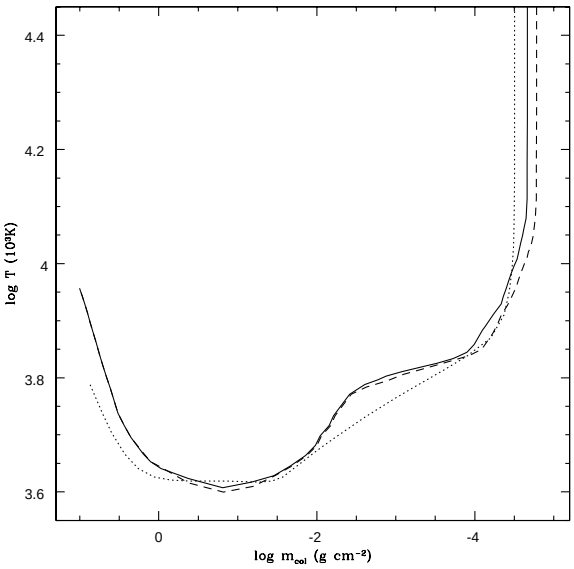

Figure 2. Models for ε Eri in its minimum (dashed line) and its maximum situation (full line). For comparison, we show the model B from Sim & Jordan (2005) (dotted line)

comparison of the observed and computed profiles for both levels of activity. It is important to note the good agreement of the fit, even better than the one by Thatcher et al. (1991) for all the diagnostic lines and continuum.

On top of the chromosphere, we added a transition region with a similar structure to the solar one. Since we have no observations of lines formed in this region, we could no constrain it further. However, the position at which the transition region begins was adjusted to fit the observed emission of the Ca II k line.

There are several differences between our model and the one by SJ05. In our model, the photosphere is hotter, the temperature minimum region is narrower and the chromospheric rise has a larger slope. Also, their transition region is placed deeper in the atmosphere, *i.e.*, at higher values of the column mass.

The differences between these models may be caused by several factors. As we have already noted, SJ05 used a higher value of surface gravity which could explain the differences in all the thermal structure. The differences in the photospheric structure could arise from the fact that we used the complete spectra to fit the continuum emission, and SJ05 used the photospheric model by Thatcher et al. (1991), built to fit only the Ca II K line wings, which are formed in the higher photosphere.

Another important factor to consider is the moment of the activity cycle in which the observations used to build the model were taken. In our case, all the lines used as diagnostics correspond to the same activity level since they were all observed simultaneously. But in the model by SJ05, the structure of the higher chromosphere and transition region was assembled with the model by Thatcher et al. (1991) for the lower chromosphere and photosphere, whitout taking into account that these thermal structures were obtained using line profiles that correspond to different parts of the

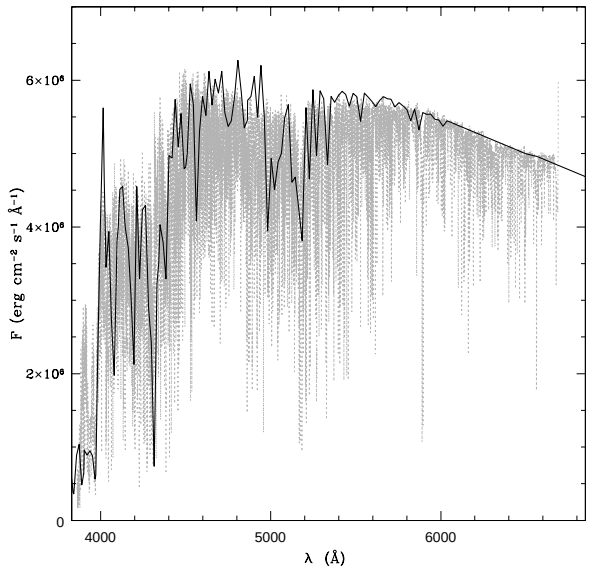

Figure 3. Comparison between the observed (grey) and computed continuum (black) for ε Eri.

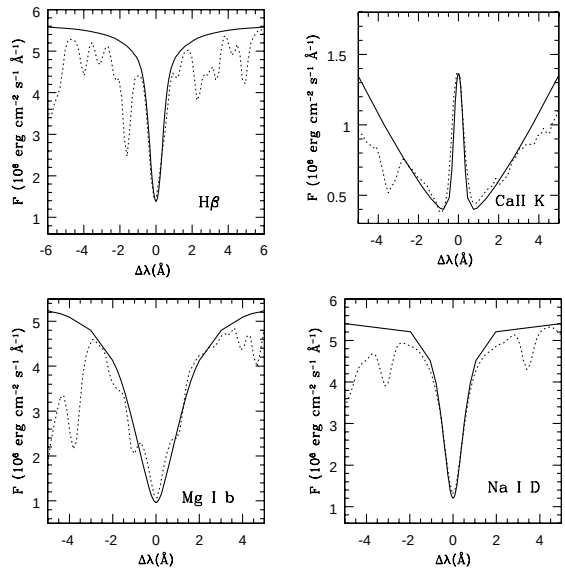

Figure 4. Comparison of observed (dashed line) and computed profiles (full line) for ε Eri in its minimum.

activity cycle. For these reasons, the comparison between these models is only qualitative.

Regarding the differences in the atmospheric structure between the maximum and the minimum level of activity, the changes occur all along the atmosphere (Figure 2), from the temperature minimum to the transition region. The position of the minimum is the same in both situations, although the temperature increases from 3980 K to 4050 K.

Finally, to check whether our results are affected by the adopted value of the metallicity, we computed the emitted profiles for our models with the metallicity given by Zhao et al. (2002), which was used by Ness & Jordan (2008), and we found no significant differences, which is consistent with the results obtained by Ayres & Linsky (1976).

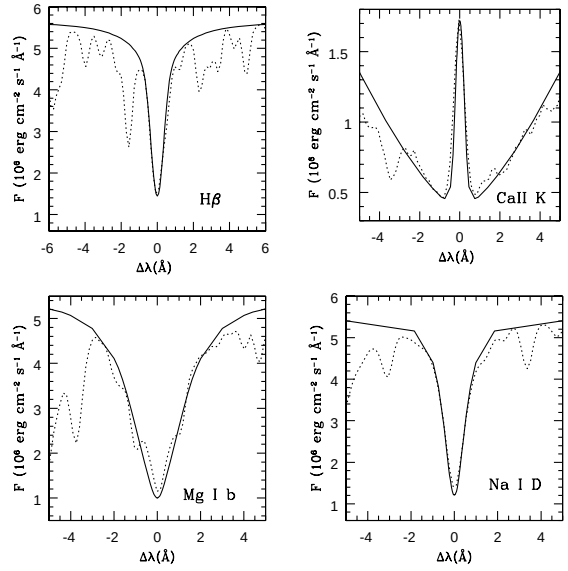

Figure 5. Comparison of observed (dashed line) and computed profiles (full line) for ε Eri in its maximum.

3.3 The other stars

To build the models for the other stars in the sample, we used solar metallicity and the same surface gravity that was used for ε Eri. The stellar surface flux was computed with Equation 2, using for each star the $T_{\rm eff}$ values shown in Table 2. Since we want to study the changes in thermal structure induced by activity, we made the approximation that all the stars have the same photosphere than ε Eri.

The models for the less active stars (HD 128621 and HD 26965 in its maximum and minimum activity level, and ε Eri in its minimum) are shown in Figure 6. It can be seen that all these models have the temperature minimum between 60 and 100 km higher, and from 20 to 240 K cooler that ε Eri in its minimum.

The temperature in the chromosphere, from the temperature-minimum region up to 1100 km, increases with activity, although the largest differences are in the chromospheric plateau. These changes with activity are different to those obtained for G stars (Paper I) with similar activity levels, because in that case only the temperature minimum region changed, and the rest of the atmospheric structure remained the same.

An important fact which can be seen in Figure 6, is that the differences in the atmospheric structure for a star in its maximum and minimum activity levels are comparable to the changes seen beetwen two different stars. This fact stresses how important it is, when building an atmospheric model, the moment at which the observations to be ajusted are made, and, in particular, how important it is to use simultaneous observations of the diagnostic lines.

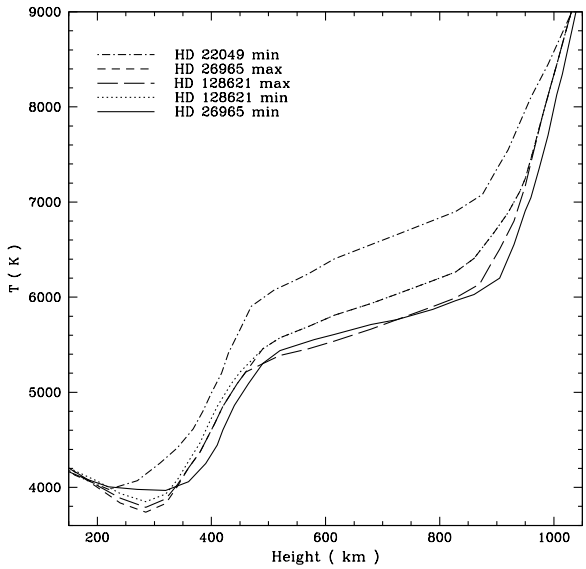

Figure 6. Models for the less active group. All the models have the same structure below 150 km.

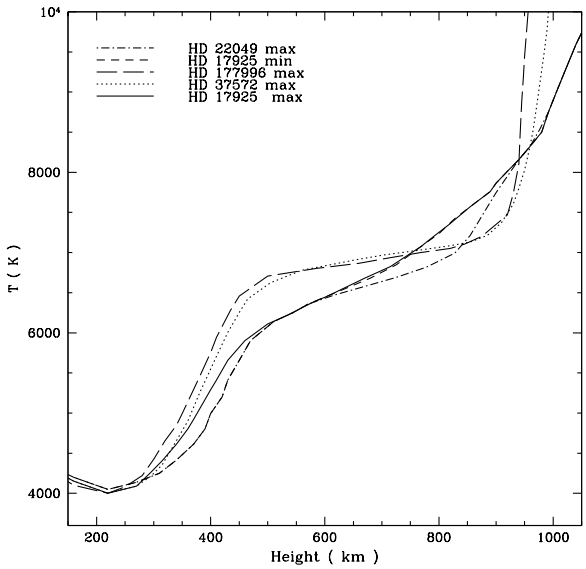

Figure 7. Models for the more active group. All the models have the same structure below 150 km.

In Figure 13 to 16 we show the observed and computed profiles for α Cen B (HD 128621) and HD 26965 in its maximum and minimum states. It is important to note the change in scale to compare with Figures 4 and 5, since these two stars are less active than ε Eridani.

The models for the most active stars (HD 17925 in both activity levels, and HD 22049, HD 37572 and HD 177996 in their maximum) are shown in Figure 7. Again the differences in the atmospheric structure for a star in its maximum and minimum activity levels are similar to the changes seen beetwen two different stars.

In Figure 7 it can be seen that for the stars in this group the temperature minimum is hotter than for the stars in Figure 6, and this temperature is almost constant as the activity level increases, varying only 50 K. The position of this region is also the same for all these stars. The atmospheric structure changes with activity everywhere in the chromosphere, mainly in the plateau and the rise to the transition region.

The observed and synthetic profiles for the most active stars are compared in Figures 17 to 20. Again, it is important to note the change in the scale for comparison with the lesser active stars and the good fit in all cases.

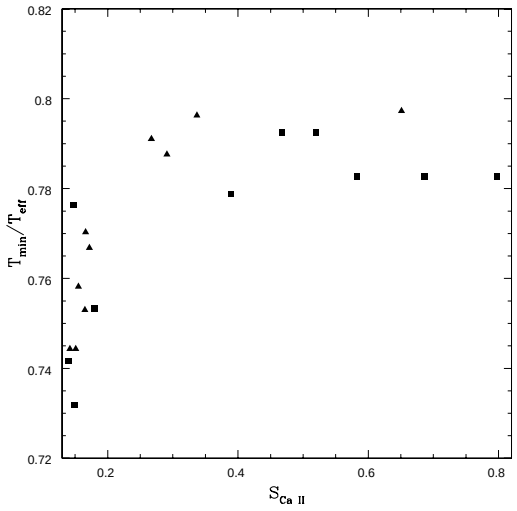

Figure 8. $T_{\rm min}/T_{\rm eff}$ vs. $S_{\rm CaII}$ **computed from the models** for K stars (this paper, squares) and for G stars (Paper I, triangles).

4 NON-RADIATIVE HEATING IN K STARS

As was mentioned in Kelch et al. (1979), the ratio of the temperature in the minimum and the effective temperature ($T_{\rm min}/T_{\rm eff}$) gives an indication of the importance of nonradiative heating in the upper photosphere of stars. There, they compare this ratio with $T_{\rm eff}$ to study the trend due to spectral type.

In Figure 8 we plot this ratio versus $S_{\rm CaII}$, which is an indicator of the level of magnetic activity in the chromosphere for all stars independently of spectral type. The values of $S_{\rm CaII}$ were obtained by integration of the synthetic profiles, and in the figure we include the values obtained from the models for K stars built in this paper and those for G stars constructed in Paper I.

In the figure it is possible to observe that there is a saturation in $T_{\rm min}$. In fact, its value increases with activity up to $T_{\rm min}/T_{\rm eff} \sim 0.79$, and after that it remains almost constant even if activity increases further. On the other hand, the computed value of $T_{\rm min}/T_{\rm eff}$ for G stars is larger than for K stars with similar activity levels.

In Figure 9 (left) we show the position of the temperature minimum region in column mass as a function of $S_{\rm CaII}$ for G (Paper I, triangles) and K stars (squares). For K stars the temperature minimum occurs deeper than for G stars, and there is a tendency for this region to move inward as activity grows. In other words, the temperature inversion oc-

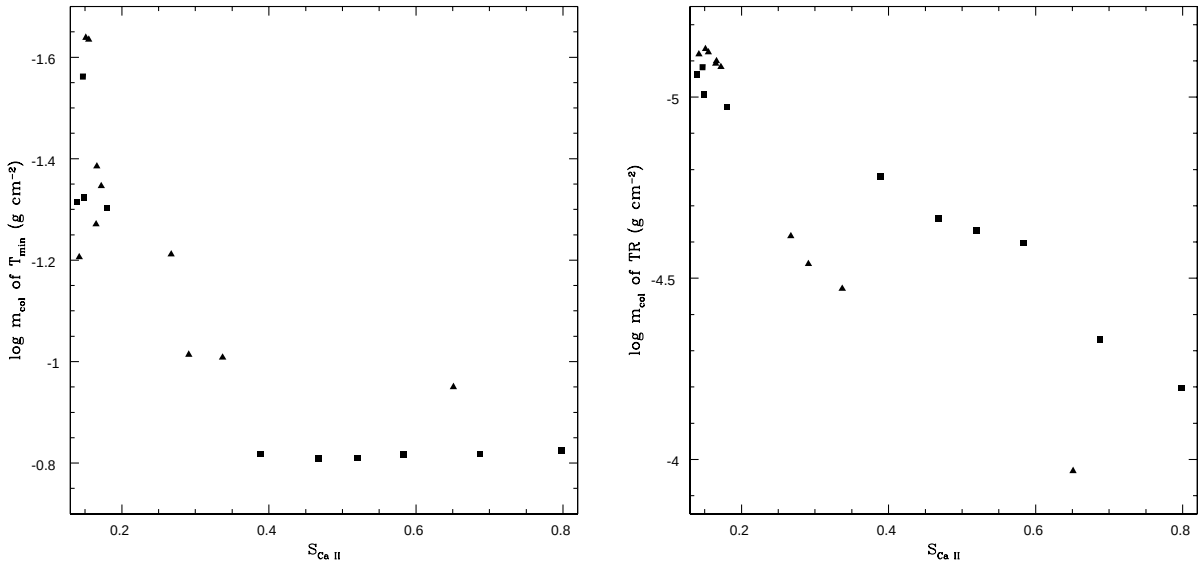

Figure 9. Position (in column mass) of the temperature minimum region (left) and the transition region (right), as a function of **computed** S_{CaII} for G (Paper I, triangles) and K stars (squares).

curs deeper for more active stars, indicating that the energy deposition starts deeper in the atmosphere as the activity level increases, for both spectral types. In Figure 9 we also show the position of the transition region (TR), specifically the height at which the temperature reaches 36000 K. It can be seen that for G stars the chromosphere is more extended than for K stars, and that in both cases the TR moves inward as activity increases.

To study the energetic requirements to maintain the atmospheric structure, we calculated the total net radiative loss for each model in the same way as in Paper I. At a given depth, the radiative cooling rate Φ (ergs cm^{-3} sec^{-1}) in a given spectral feature (line or continuum) can be computed as (Vernazza et al. 1981)

$$\Phi = 4\pi \int \kappa_\nu \, (S_\nu - J_\nu) \, d\nu \, , \qquad (3)$$

where S_ν is the source function and J_ν is the mean intensity at frequency ν. A positive value of Φ implies a net loss of energy (cooling), and a negative value represents a net energy absorption.

Here, we considered line and continua of H, H-, H-ff, Mg I and II, Fe I, Si I, Ca II, Na I and CO. The total rates for each star are shown in Figure 10 for the less active models, and in Figure 11 for the more active ones. As it is expected, the amount of non-radiative energy supplied to the chromosphere increases everywhere with magnetic activity.

In both figures, it is possible to note a region where the net cooling rate is negative. This result has already been found for G stars in Paper I, for which a negative cooling rate in the temperature minimum region was also obtained. This fact have been already shown for the Sun (Vernazza et al. 1981). Within the plane-parallel, homogeneous approximation we are investigating, this implies either mechanical energy extraction or, more likely, that the calculations have neglected important sources of radiative cooling (see Mauas 1993).

The main contributions in this zone are H-, Si I, Fe I and CO, the same than for G stars. It is important to note that since the temperature for K stars is lower in this region, there could be an important contribution of several molecules which we do not consider in our calculations, like, for example, CH, that could act as cooling agents. Considering these contributions could bring our computations closer to energy balance.

For the less active models the cooling rate becomes positive at around 300 km, implying that there is mechanical energy deposition above this height. For the most active models, this energy deposition starts deeper in the atmosphere, *i.e.* the chromosphere starts deeper.

Also in the chromosphere, the most important contributors to the cooling rate are the same than for G stars, but the proportions are different: for ε Eri in its minimum, for example, Mg II and Ca II contribute with $\sim 9\%$ each, while for the Sun these contributions are of $\sim 20\%$. The contribution by Fe I, on the other hand, is of $\sim 15\%$ in ε Eri, but only $\sim 10\%$ in the Sun. In both cases, almost half of the total cooling rate corresponds to line blanketing.

Finally, to quantify the total amount of mechanical energy deposited in the chromosphere, we integrated the net radiative cooling rate from the depth in the chromosphere where the cooling rate becomes positive to the region where the temperature reaches 10^4 K. To compare the results for both spectral types, we normalized the resulting quantity, $\phi_{\rm int}$, by the surface luminosity ($\sigma T_{\rm eff}^4$) **The resulting quantity, therefore, gives an idea of the fraction of the total energy emitted by the star that goes into heating the chromosphere.** The results are shown in Figure 12, where it can be seen that there is a unique trend for all stars, independently of spectral type. This fact seems to imply that the physical processes that supply the energy to

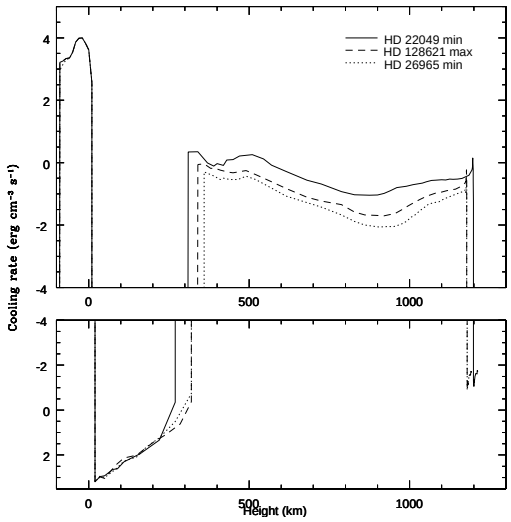

Figure 10. Total cooling rate for the less active stars.

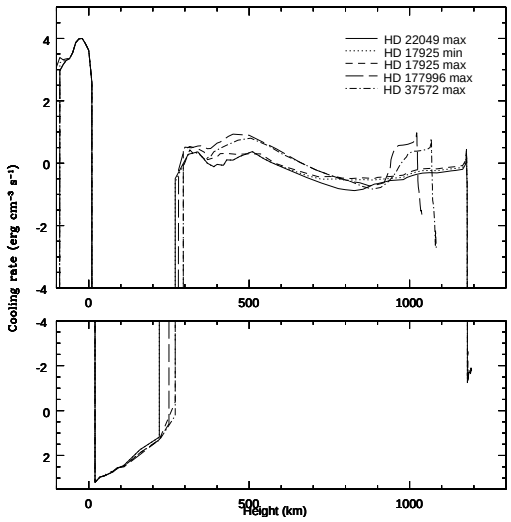

Figure 11. Total cooling rate for the more active stars.

sustain the atmospheric structure are independent of spectral type.

Given the good relation between S_{CaII} and the normalized ϕ_{int}, we fit the data with a polynomial function, given by

$$\frac{\phi_{\rm int}}{\sigma T_{\rm eff}^4} = -1.14\ 10^{-5} + 1.28\ 10^{-4}\ S_{\rm CaII} + 2.80\ 10^{-4}\ S_{\rm CaII}^2 - 2.80\ 10^{-4}\ S_{\rm CaII}^3\ . \quad (4)$$

In Figure 12 it can be seen that the fit is very good and, therefore, the energetic requirements of a given star can be estimated from its chromospheric activity level as mesured by S_{CaII}.

5 DISCUSSION

One of the main goals of chromospheric modelling is to accurately estimate the radiative losses in the chromosphere

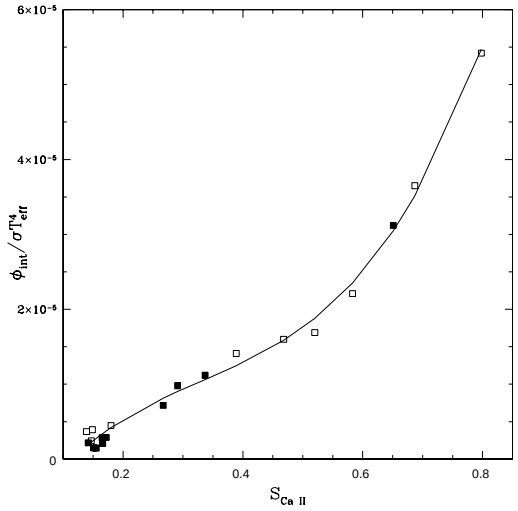

Figure 12. Normalized $\phi_{\rm int}$ versus **computed** S_{CaII} index. **Empty** squares represent the K star models from this work and **full squares** indicate the G star models from Paper I.

in detail, using only the information that can be obtained from the observations, without any assumption about the physical processes involved. In this way, these losses can be equaled to the energy requirements that any proposed mechanism of chromospheric heating should match.

For example, we saw in the previous section that the contribution of the different features to the total cooling rate is not the same for G and K stars. In particular, the Ca II, Mg II and Fe I relative contributions are not the same for both spectral types. Therefore, it might not be correct to scale the relative contributions computed for the Sun to K stars, as it has been done sometimes (see Cuntz et al. 1999, and Rammacher et al. 2005).

Cuntz et al. (1999) computed theoretical two-component models for K dwarfs of different activity levels. They proposed that the energy is deposited in the chromosphere by acoustic and magnetic shocks, and found that these shocks are stronger and are produced deeper in the chromosphere as the activity of the star increases. This result is in agreement with our calculations, which shows that the energy deposition is larger and deposited deeper with increasing activity.

On the other hand, they reproduced the lineal trend between the Ca II H and K lines fluxes and the rotational period, although their computed fluxes are smaller than the observations, which could again be due to their sketchy calculation of the radiative cooling rate.

6 SUMMARY

In this paper we present chromospheric models for six K dwarfs, including ε Eridani, with similar photospheric properties but different magnetic activity levels. In several cases we computed models for two moments of the activity cycle for the same star.

These models were based on, and reproduced very well, the Ca II H and K and the Hβ line profiles for all the stars in

our sample. The reliability of the stellar atmospheric models was checked with other features, the Na I D and Mg I b lines. Also for these lines we found very good agreement between computed and observed profiles.

We found that the changes in atmospheric structure in K dwarfs with activity are produced all along the chromosphere, from the region of the temperature minimum to the transition region and mainly in the chromospheric plateau, independently of the activity level of the star. This was not the case for the G dwarfs modelled in Paper I, since for the less active G stars the changes with activity occur only in the region of the temperature minimum.

The ratio of the minimum and effective temperatures ($T_{\rm min}/T_{\rm eff}$) can give an idea of the importance of non-radiative heating in the upper photosphere of stars. Both for K and G stars, this value increases with activity up to $T_{\rm min}/T_{\rm eff} \sim 0.79$, where it saturates, and it remains constant even if the activity level increases further. On the other hand, the computed value of $T_{\rm min}/T_{\rm eff}$ for G stars is larger than for K stars with similar activity.

For both spectral types, the position of the temperature minimum moves inward as activity increases, implying that the chromosphere starts deeper in more active stars. This, in turn, implies that as the activity level increases, the energy deposition occurs deeper in the atmosphere.

On the other hand, the transition region is placed at higher column masses for G stars than for K stars, and in both cases it moves inward as activity increases.

Regarding the energetic requirements, the integrated chromospheric radiative losses, normalized to the surface luminosity, show a unique trend for G and K dwarfs when plotted against $S_{\rm CaII}$, the main proxy of stellar activity. This might indicate that the same physical processes are heating the stellar chromospheres in both cases. We calculated an empirical relationship between the $S_{\rm CaII}$ index and the energy deposited in the chromosphere, which can be used to estimate the energetic requirements of a given star knowing its chromospheric activity level.

There are significant differences in the contributions of Mg II, Ca II and Fe I to the total net cooling rate in the chromosphere between G and K stars, which implies that values obtained for a given star should not be extrapolated to another one of a different spectral type, as usually is done. In both cases about half of the total rate is due to line blanketing.

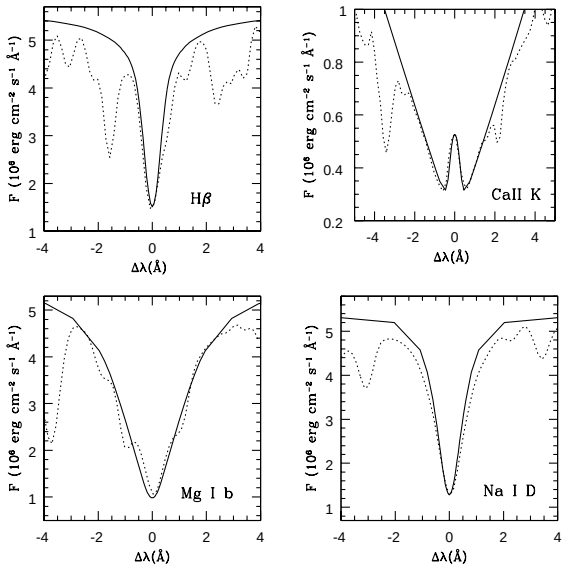

Figure 13. Comparison of observed (dashed line) and computed profiles (full line) for α Cen B (HD 128621) in its maximum.

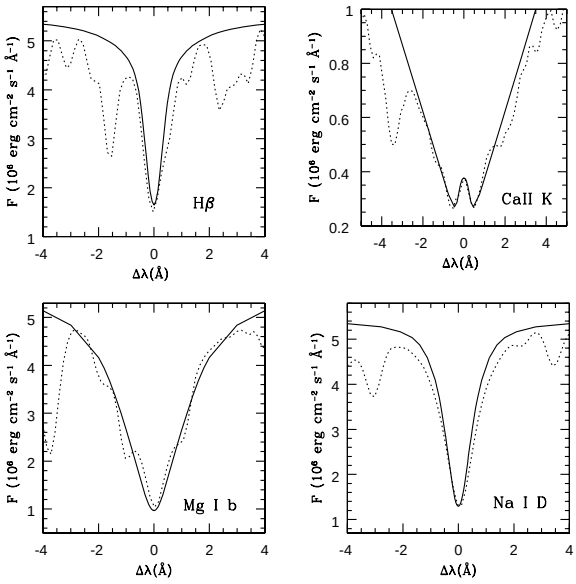

Figure 14. Comparison of observed (dashed line) and computed profiles (full line) for α Cen B (HD 128621) in its minimum.

ACKNOWLEDGMENTS

We would like to thank the director of the CASLEO Observatory, and all the staff of this institution. The CCD and data acquisition system at CASLEO has been partly financed by R.M. Rich through U.S. NSF grant AST-90-15827. We also than the anonymous referee, whose comments help us to improve this paper. This work made extensive use of the SIMBAD database, operated at CDS, Strasbourg, France.

REFERENCES

Abia, C., Rebolo, R., Beckman, J. E., & Crivellari, L. 1988, A&A, 206, 100

Allende Prieto, C., Barklem, P., Lambert, D., & Cunha, K. 2004, A&A, 420, 183

Anderson L. S. 1989, ApJ, 339, 558

Avrett E., & Loeser R. 2003, in Modeling of Stellar Atmospheres, IAU Symp. No. 210, ed. W. Weiss & N. Piskunov (Dordrecht: Kluwer), A-21

Ayres, T.R. 1981, ApJ 244, 1064

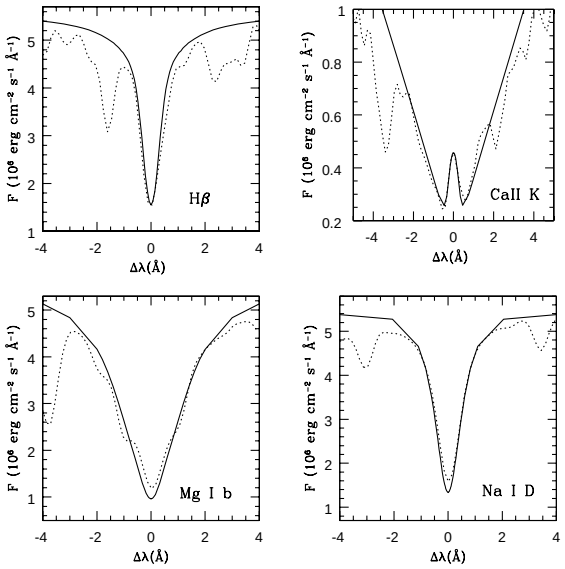

Figure 15. Comparison of observed (dashed line) and computed profiles (full line) for HD 26965 in its maximum.

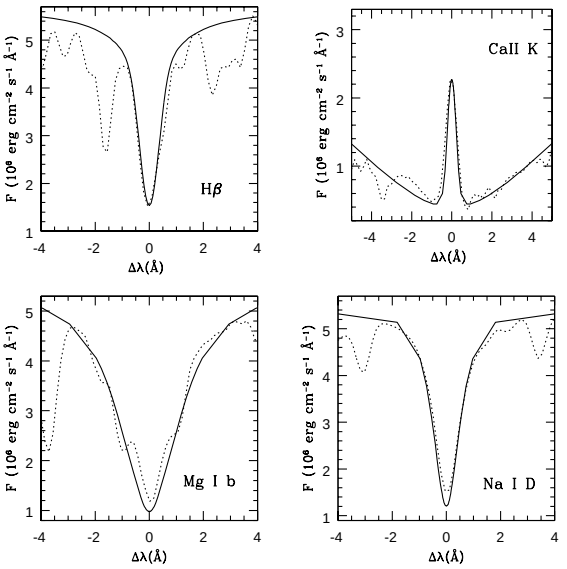

Figure 17. Comparison of observed (dashed line) and computed profiles (full line) for HD 17925 in its maximum.

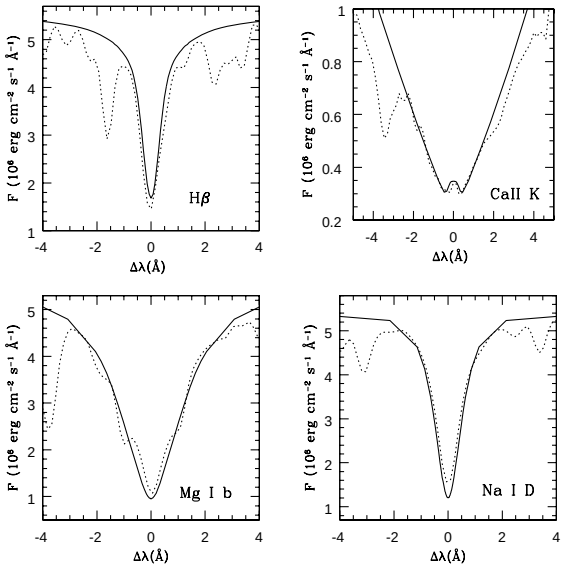

Figure 16. Comparison of observed (dashed line) and computed profiles (full line) for HD 26965 in its minimum.

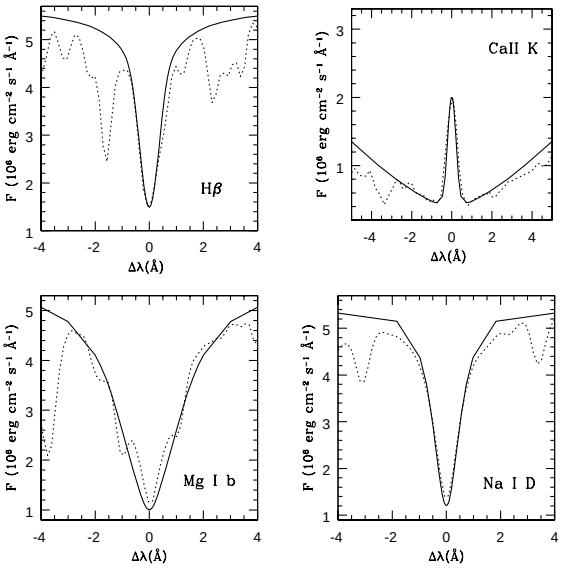

Figure 18. Comparison of observed (dashed line) and computed profiles (full line) for HD 17925 in its minimum.

Ayres T., & Linsky J. 1976, ApJ, 210, 199
Bell, R. A., & Gustafsson, B. 1989, MNRAS, 221, 427
Bodaghee, A., Santos, N. C., Israelian, G., & Mayor, M. 2003, A&A, 404, 715
Bohm-Vitense, E. 1981, ARAA, 23, 319
Buccino, A., & Mauas, P. 2008, A&A, 483, 903
Burnashev, V. I. 1983, Izv. Krym. Astrofiz. Obs., 67, 13
Cayrel de Strobel G., Soubiran C., Ralite N. 2001, A&A, 373, 159
Cincunegui C., & Mauas P. 2004, A&A, 414, 699
Cincunegui, C.C., Diaz, R., Mauas, P.J.D. 2007, A&A 469, 309
Cox, A., 2000, Allen's Astrophysical Quantities, fourth edition (Springer-Verlag), p. 389
Cuntz, M. Rammacher, W., Ulmschneider, P., Musielak, Z. E.,& Saar, S. H. 1999, ApJ, 522, 1053
Díaz, R. F., Cincunegui, C., & Mauas, P. J. D 2007, MNRAS, 378, 1007
Drake, J., & Smith, G. 1993, ApJ, 412, 809
Eggenberger, P., Charbonnel, C., Talon, S., Maynet, G., Carrier, F., & Bourban, G., 2004, A&A, 417, 235
Falchi, A., & Mauas, P.J.D. 1998, A&A, 336, 281

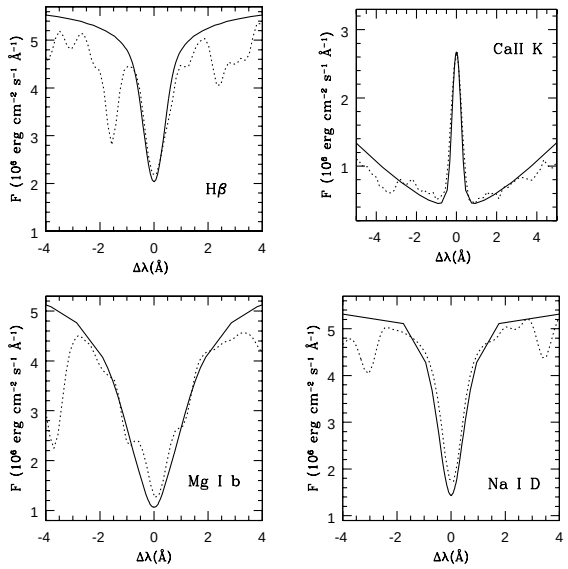

Figure 19. Comparison of observed (dashed line) and computed profiles (full line) for HD 37572 in its maximum.

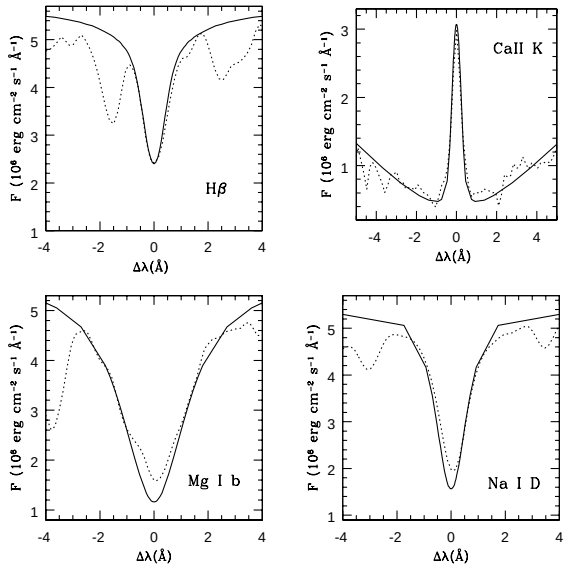

Figure 20. Comparison of observed (dashed line) and computed profiles (full line) for HD 177996.

Fontenla, J., Avrett, E., & Loeser, R. 1993, ApJ, 406, 319
Guenther, D., & Demarque, P., 2000, ApJ, 531, 503
Gustafsson, B., Bell, R., Eriksson, K., & Nordlund, A., 1975, A&A, 42, 407
Henry T., Soderblom D., Donahue R., & Baliunas S. 1996, AJ, 111, 439
Hearnshaw, J. B. 1998, A&A, 34, 263
Johnson, H. L., Iriarte, B., Mitchell, R. I., & Wisniewskj, W. Z., 1966 Comm. Lunar Plan. Lab., 4, 99
Kelch, W.L 1978, ApJ, 222, 931
Kelch, W.L, Worden, S. P., & Linsky, J. L. 1979, ApJ, 229, 700
Krishna Swamy,K. S. 1966, ApJ, 145, 174
Linsky, J. L. & Ayres, T. R. 1979, ApJ, 220, 619
Mallik, S.1998, A&A, 338, 623
Mauas, P. J., Avrett, E. H., & Loeser, R. 1988, ApJ 330, 1008
Mauas, P.J.D., Avrett, E.H., Loeser, R. 1990a, ApJ 357, 279
Mauas P.J.D. 1993, ApJ, 414, 928
Mauas P.J.D., Falchi A. 1994, A&A, 281, 129
Mauas P.J.D. & Falchi A. 1996, A&A, 310, 245
Mauas P.J.D., Falchi A., Pasquini L., & Pallavicini R. 1997, A&A, 326, 256
Ness, J., Jordan, C. 2008, MNRAS, 385, 1691
Oinas, V. 1974, ApJS, 27, 405
Perryman, M. A. C., Lindegren, L., Kovalevsky, J., et al. 1997, A&A, 323, L49
Rammacher, W., Fawzy, D., Ulmschneider, P., & Musielak, Z. 2005, ApJ, 631, 1113
Schmidt-Kaler, Th. 1982, Landolt-Bornsterin series, Numerical Data and Funcional Relationships in Science and Technology, Group VI, Vol. 2b, eds. K. Schaifers, H. H. Voigt (Springer-Verlag), p.451
Sim, S. A., & Jordan, C. 2005, MNRAS, 361, 1102
Simon, T., Kelch, W., & Linsky, J. 1980, ApJ, 237, 72
Steenbock W. 1983, A&A, 126, 325
Steenbock W., & Holweger, H. 1981, A&A, 99, 192
Thatcher, J., Robinson, R., & Rees, D. 1991, MNRAS, 250, 14
Tomkin, J., & Lambert, D. 1999, ApJ, 523, 234
Tomkin, J., & Lambert, D. 1980, ApJ, 334, 1008
Ulmschneider, P., & Musielak, Z. 2003, ASPC, 286, 363
Vaughan, A. H., Preston, G. W. & Wilson, O. C 1978, PASP, 90, 267
Vernazza J., Avrett E., & Loeser R. 1981, ApJS, 45, 635
Vieytes, M., Mauas, P., & Cincunegui, C. 2005, A&A, 441, 701 (Paper I)
Wedemeyer-Bohm, S.; Steffen, M. 2007, A&A, 462, L31
Zhao, G., Chen, Y., Qiu, H., & Li, Z. 2002, ApJ, 124, 2224